Channel Sounding System for MM-Wave Bands and Characterization of Indoor Propagation at 28 GHz

Hejselbæk, Johannes; Ji, Yilin; Fan, Wei; Pedersen, Gert F.

Published in:
International Journal of Wireless Information Networks

DOI (link to publication from Publisher):
10.1007/s10776-017-0365-0

Publication date:
2017

Document Version
Accepted author manuscript, peer reviewed version

Channel Sounding System for mm-Wave Bands and Characterization of Indoor Propagation at 28 GHz

Journal:
International Journal of Wireless Information Networks

Date submitted by the author:
First submitted: 7-Jan-2017 - Revised version submitted: 23-may-2017

List of author(s) with affiliation(s):
Johannes Hejselbaek; Aalborg University, Department of Electronic Systems (ORCID - 0000-0002-3053-5474)
Yilin Ji; Aalborg University, Department of Electronic Systems (ORCID - 0000-0003-4072-9392)
Wei Fan; Aalborg University, Department of Electronic Systems (ORCID - 0000-0002-9835-4485)
Gert F. Pedersen; Aalborg University, Department of Electronic Systems (ORCID - 0000-0002-6570-7387)

Corresponding author:
Wei Fan
Aalborg University, Department of Electronic Systems
Niels Jernes Vej 12
9220 Aalborg Ost, Denmark
Phone: +45 22326957
Email: wfa@es.aau.dk

Notes to the editor:
Invited paper from PIMRC16, intended for special issue on selected topics within Millimeter-wave and Massive MIMO Radio Communications for 5G.

PIMRC paper information:
J. Hejselbaek, W. Fan, and G. F. Pedersen, Ultrawideband vna based channel sounding system for centimetre and millimetre wave bands, in 2016 IEEE 27th Annual International Symposium on Personal, Indoor, and Mobile Radio Communications (PIMRC), Sept 2016, pp. 16.

International Journal of Wireless Information Networks, manuscript No.
(will be inserted by the editor)

Channel Sounding System for mm-Wave Bands and Characterization of Indoor Propagation at 28 GHz

Johannes Hejselbaek · Yilin Ji · Wei Fan · Gert F. Pedersen

Received: 7-Jan-2017 / Accepted: 7-Jul-2017

Abstract The aim of this work is to present a vector network analyzer (VNA) based channel sounding system capable of performing measurements in the range from 2 to 50 GHz. Further, this paper describes an indoor measurement camOkipaign performed at 26 to 30 GHz. The sounding system is capable of receiving two channels and transmitting one. Using this feature a channel measurement has been performed using both a directional horn antenna and a virtual uniform circular array (UCA) at the same time. This allows for comparative studies of measured channels with two different antennas in a simultaneous way. The measurement has been conducted with 42 measurement positions distributed along a 10 m long path through an indoor laboratory environment. The transmitter was positioned such that measurements were conducted both in line-of-sight (LOS) and non-line-of-sight (NLOS) scenarios.

The measurements showed good agreement between the measurement data collected with the horn antenna and the data collected with the UCA. The propagation environment was found to be sparse both in delay and angular domain for the given scenario. Based on the performed measurement campaign together with validation measurements of the system stability, it is found that the system works as expected.

Keywords Radio Wave Propagation · Multipath Channels · Angular Power Spectrum · Channel Sounding · Centimetre and Millimetre Wave Bands

The work have been conducted under the framework of the VIRTUOSO project. The Danish National Advanced Technology Foundation supports this project together with industry partners.

Johannes Hejselbaek
APNet, Aalborg University
E-mail: joh@es.aau.dk

Yilin Ji
APNet, Aalborg University
E-mail: yilin@es.aau.dk

Wei Fan
APNet, Aalborg University
E-mail: wfa@es.aau.dk

Gert. F. Pedersen
APNet, Aalborg University
E-mail: gfp@es.aau.dk

1 Introduction

The increasing growth in demand for mobile data is one of the driving factors for the industry in moving towards a fifth generation mobile communication network (5G) [1,2]. To help facilitate the demand, there is a need for unused radio spectrum, which is scarce below 6 GHz. The available spectrum of interest, which ranges from 6 GHz to 100 GHz, falls in the two bands denoted the super-high-frequency (SHF) band (3 - 30 GHz) and the extremely high-frequency (EHF) band (30 - 300 GHz). These are also referred to as the centimetre and millimetre wave bands. In this large range from 6 GHz to 100 GHz, multiple frequency bands have been suggested as candidates for 5G [2–5]. The studies point out that for larger area coverage the lower frequencies are preferable due to the frequency dependent free-space path-loss together with other physical constraints such as atmospheric attenuation. As an example, high oxygen absorption is seen at 60 GHz used for IEEE 802.11ad (WLAN) [6]. As a result, the frequency range from 15 GHz to 40 GHz which are expected to be more suitable for cellular communication has received the most attention in regards to channel measurements [7–15].

These studies mainly focus on path-loss, the angle of arrival (AoA) and the delay-spread (DS) in static or

quasi-static environments. Especially the AoA has been of interest as the angular information is needed to facilitate beam forming, which is seen as one of the key enabling technologies for 5G [3, 16]. The suggested use of high frequencies for 5G systems enables the implementation of massive antenna arrays due to the small antenna elements. This allows for utilization of the spatial dimension via e.g., beamforming algorithms, which can improve the system performance in signal strength levels significantly and thereby data [17,18]. Therefore, a study of the AoAs in the given propagation environments is the focus of this paper.

Generally two different types of channel sounding systems are widely utilized in the literature, namely time-domain and frequency-domain sounders [19]. The time-domain sounders utilize a transmitted pseudo random binary sequence (PRBS) which is recovered by a correlative process. This requires dedicated equipment specially build for the purpose. The correlative channel sounders are capable of recovering an estimate of the channel impulse response (CIR) very fast and are therefore preferable for measurements of the dynamic propagation environment [20,21]. However, the complexity of generating and sampling the PRBS poses challenges if a large bandwidth is of interest [20]. Nevertheless, have bandwidths of up to 6 GHz been reported in [22, 23]. The frequency-domain sounders sweep the chosen frequency band with a continuous wave (CW). Due to this frequency sweep sounders does not have the same constraints in the measurable bandwidth as for the correlative channel. The limiting factor then becomes the acceptable measurement time as the frequency sweep time has to be considered. For a static propagation environment, this is not a problem but if a dynamic environment is to be measured this has to be considered. A method to overcome this is to use very fast frequency sweeping systems known as frequency modulated continuous wave (FMCW) or chirp sounders. These have been reported in literature also with a bandwidth of up to 6 GHz for capable of measuring in a dynamic environment with speeds of up to 20 km/h [24,25]. However, again these system requires dedicated equipment which has to be modified for measurements in a given frequency range. It is costly and limited in availability to have dedicated equipment. Due to this, a more simple approach of utilizing a general purpose Vector Network Analyser (VNA) is often seen in literature [10,13,26]. A VNA based system sweeps the chosen frequency band while the channel frequency response is measured between two ports. The sweep time of the high precision CW generator used by the VNA is considerable higher than the one for the chirp sounders. Due to this VNA based sounding systems are often only used in static propagation environments.

This paper presents the work related to the development of a VNA based measurement system together with an investigation of the stability of this system. The capability of the developed system is further extended to allow for simultaneous recording of two channel frequency responses together with a reference frequency response from the transmitting test port of the VNA. The extended measurement system is utilized for a measurement campaign aiming at a comparative study between a channel sounding using a virtual uniform circular array (UCA) and a directive horn to record the power-angle-delay profiles (PADP). Further, the system is used for a larger indoor measurement campaign intended for highlighting multipath component evolution over different spatial positions.

The paper is organized as follows. Section II describes the VNA-based channel sounding system and presents the capabilities and limitations of the system. Section III presents the extended measurement system used for the measurements presented in Section IV. Section V summarizes this work.

2 Channel Sounding System

The VNA measurement system presented in this work is utilizing the *Agilent N5227A PNA*. To extend the physical range of the measurements, the VNA is used together with a distribution system, also from Agilent, including mixers and amplifiers. The basic principle of the distribution system is that via down-converting the cable loss of high-frequency signals can be reduced. The down-converting is obtained at the mixers by applying heterodyning. The cable-losses is the main limiting factor for the physical range of the measurement system. A block diagram of the system is depicted in Fig. 1 and it contains the following blocks.

- Vector Network Analyser (VNA)
- Distribution unit for the local oscillator and intermediate frequency
- Reference mixer
- Test mixer
- Transmit (TX) and receive (RX) antennas

The distribution unit functions as an amplifier and splitter of the LO (Local Oscillator) from the VNA to the mixers. The LO signal path is marked in blue in Fig. 1. The distribution unit also provides amplification of the IF (Intermediate Frequency) from the mixers. The IF signal path is marked in red in Fig. 1. The test mixer multiplexes the IF signal on the LO connection allowing for only one cable being needed to connect test

mixer to the distribution unit. The multiplexed LO/IF signal path is marked in orange in Fig. 1. Due to the multiplexing the distribution unit also has to provide the demultiplexing of the IF from the test mixer before the VNA.

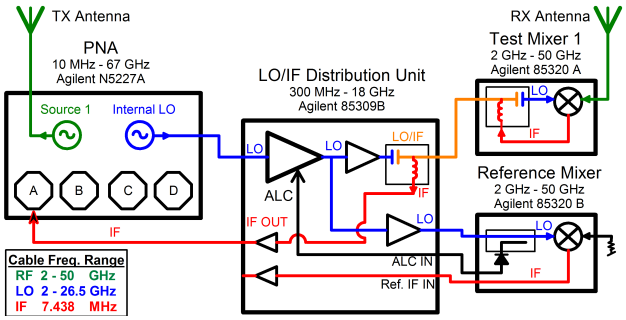

Fig. 1 Block diagram of the measurement system using internal LO. Green is RF frequency, blue is LO frequency and red is IF frequency.

The system operates with two different types of mixers, namely the test and reference mixer. The purpose of both mixers is to down-convert the received high-frequency signal to IF, which for this system is 7.438 MHz. As stated the test mixer operates with only one cable and therefore includes a multiplexer besides the down-converter. The reference mixer uses separate lines for the LO and IF and also provides feedback for the ALC (Automatic Level Control) in the distribution unit. Using the reference mixer enables the system to utilize leveled output power. A leveled output is a frequency independent output power as the frequency response of the amplifier together with the frequency dependent cable loss is corrected by adjusting the output power via the ALC. This is an important feature when large frequency ranges are measured.

2.1 Operating with internal VNA LO

The most straightforward way to utilize the LO is to use the internal LO from the VNA, as shown in Fig. 1. However, as also discussed in [27], it became evident that the used VNA only utilizes the fundamental frequency up to 26.5 GHz before it switches to the 3rd harmonics of the frequency. The distribution unit only has a frequency range from 300 MHz to 18 GHz, resulting in a lack of amplification in the range of the LO from 18 to 26.5 GHz.

To study the consequences of the mismatch between the LO of the VNA and the distribution unit amplifiers, a measurement was conducted. A frequency sweep is conducted in the range from 2 GHz to 30 GHz (1001 points). The TX port is connected directly to the test mixer input and after the manufacturer specified warm-up period a normalization/calibration is performed. The VNA is set to continuous sweeping, while the drift from the normalization is recorded. In Fig. 2 the resulting drift after 10 sweeps is presented. The power deviations up to 3 dB within 18 to 26.5 GHz is a result of the missing amplification capability of the distribution unit.

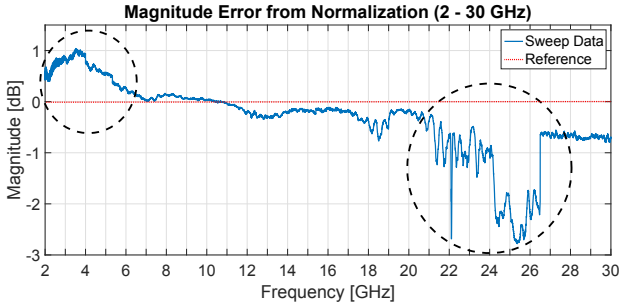

Fig. 2 Deviation from the normalization/calibration curve for the frequency sweep from 2 to 30 GHz using the internal LO.

In Fig. 2 power deviation up to 1 dB within 2 to 6 GHz is also seen. This is found to be a result of too high LO power at the test mixer. The ALC is controlled by the reference mixer and is supposed to compensate for the frequency dependent loss of the cable connecting the mixers to the distribution unit. However, in the used setup two cables of different types and lengths are used to connect the distribution unit and the two mixers. As a result, the ALC did not function as intended. A solution is simply to use the same cabling to the reference and test mixers.

2.2 Operating with alternative LO

From the presented measurement in Fig. 2 it is clear that an alternative source for the LO has to be used. The alternative source could be an external signal generator. However, the used VNA is already equipped with two source oscillators (signal generators). The benefit of using the internal source oscillators is that these can function in so-called phase lock which results in two synchronized frequency sweeps. It is possible to introduce a frequency offset between the two oscillators while maintaining phase lock as long as the two frequency ranges are of the same size. This enables the use of one oscillator (source 1) to generate the high-frequency signal for the TX antenna while the other oscillator (source 2) is used to generate the LO signal operating on a lower frequency harmonic. In Fig. 3 it can be noted that the LO is now supplied to the distribution unit from source 2 in the PNA.

The same test measurement as for the setup using the internal LO has been performed. The difference is that now source 1 is set to sweep from 2 GHz to

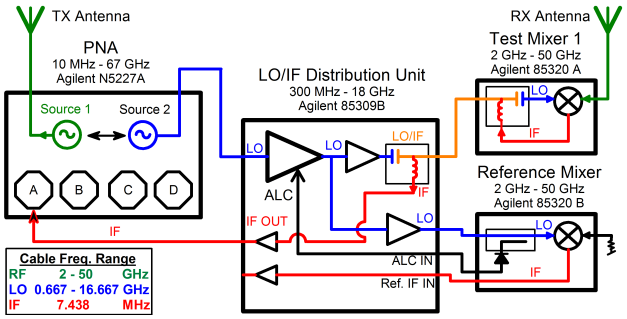

Fig. 3 Block diagram of measurement system using source 2 to generate the LO. Green is RF frequency, blue is LO frequency and red is IF frequency.

30 GHz, while source 2 is operating on the 3rd harmonic. This means that source 2 is sweeping from 2/3 GHz to 10 GHz, which ensures that the system operates within the frequency limits of the amplifiers of the distribution unit. The resulting magnitude error is shown in Fig. 4.

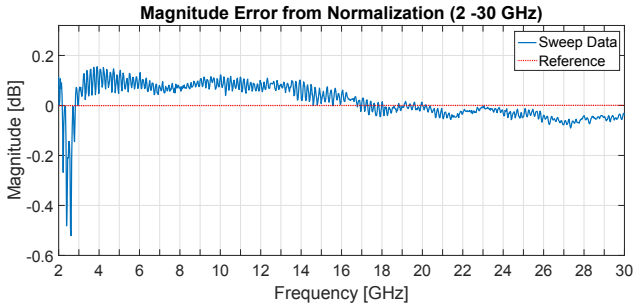

Fig. 4 Deviation from the normalization/calibration curve for the frequency sweep from 2 to 30 GHz using the alternative LO.

In Fig. 4 a significant improvement in terms of power deviations is seen when compared to Fig. 2. The only significant deviation is seen close to 2.5 GHz, which is due to the settling time of the ALC. This settling time introduces a variation of up to 0.5 dB at the low frequency. Aside from this, a variation of less than 0.1 dB is seen.

Another benefit of utilizing the 3rd harmonic is that the lowered frequency also reduces the cable losses, which can improve the operational range of the system. Lowering the frequency with higher harmonics would increase the operational range even farther. However, the use of harmonics decrease the sensitivity of the mixers and using higher harmonics will decrease the sensitivity level further.

The drift from the normalization over time is also investigated. The magnitude drift for 10 minutes, 1, 2, and 15 hours is shown in Fig. 5.

From Fig. 5 it is interesting to see that even though source 2 is used for the distribution unit and external

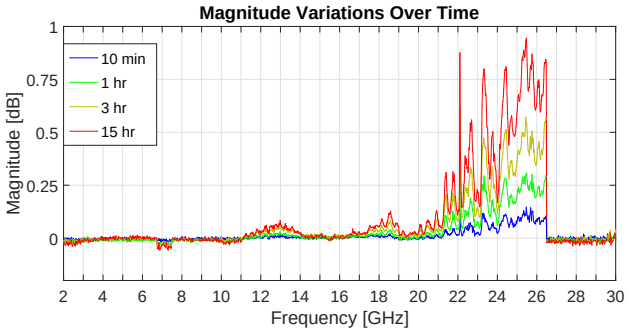

Fig. 5 Deviation over time from the normalization/calibration curve for the frequency sweep from 2 to 30 GHz using the alternative LO.

mixing, it seems that the internal LO is still problematic in the range from 21 to 26.5 GHz. The magnitude error is, however, less than 1 dB over 15 hours. If in some cases the measurement time is to exceed this long time period or the system is left for an extended period, it is clear that a new normalization/calibration has to be performed.

The phase stability of the measurement system is also investigated. The resulting plot for the unwrapped phase drift for 10 minutes, 1, 2, and 15 hours is presented in Fig. 6.

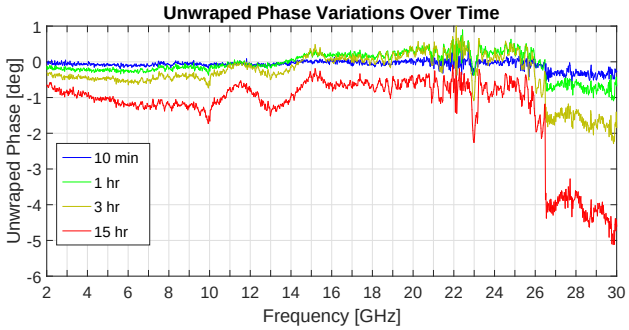

Fig. 6 Deviation from the normalization/calibration curve for the frequency sweep from 2 to 30 GHz using the alternative LO.

The unwrapped phase plotted in Fig. 6 also only shows small deviation over the extended period. For the part of the frequency sweep where the internal LO is running on the fundamental frequency the deviation less than 1^o. At the shift point for the internal LO harmonic shift point, a jump in the phase is seen. At the 15 hours sweep the jump is roughly 4^o but it seems the phase stabilizes again after the jump. As for the variation in magnitude, the phase variations is also tolerable.

The presented measurement of phase variations was conducted without moving the connected cables. Phase change due to cable movement while conducting high-frequency measurements is a known problem especially

at higher frequencies. This is also a reason for down-converting the LO signal as this would make the system less sensitive to movement of the cables. However, using higher harmonics would, as mentioned, decrease the sensitivity level of the mixers which is also an unwanted effect. Therefore, to decrees the impact of the phase changes introduced by the cables much care have to be given to minimize movement of the cable while measurements are conducted.

2.3 System link budget

The system link budget is important to ensure the RF power requirements of the used equipment. This link budget is not to be confused with the in-the-air propagation loss, as it only factors the RF chain losses. The physical range of a VNA measurement system is mainly limited by the power requirements to the distributed LO. Therefore the focus of this system link budget is the LO power loses tolerable to obtain the maximum physical measurement range.

The used test mixers have a frequency range from 2 to 50 GHz and the lowest detectable RF input at the test mixers is given by their sensitivity level. The power requirement for the test mixers LO input is between +12 and +17 dBm. If this power requirement is met, the sensitivity level, when operating the test mixers with 3rd harmonic, is -118 dBm for 2 GHz to 18 GHz, -103 dBm for 18 GHz to 40 GHz and -100 dBm for 40 GHz to 50 GHz, respectively. The aim is then to ensure the correct power level of the LO input to the test mixer. When making the link budget the most critical case, at the highest frequency, has to be used for the loss calculations. As an example, the calculations for 30 GHz is presented here. The 3rd harmonic of 30 GHz is simply 10 GHz and according to the specifications, the maximum LO output power from the distribution unit is +23.5 dBm in the frequency range from 6.2 to 18 GHz. This is on the condition that the distribution unit is given an LO input signal of +6 dBm from the VNA. This leaves $23.5 - 12 = 11.5$ dB for cable loss between distribution unit and mixer as illustrated in Fig. 7.

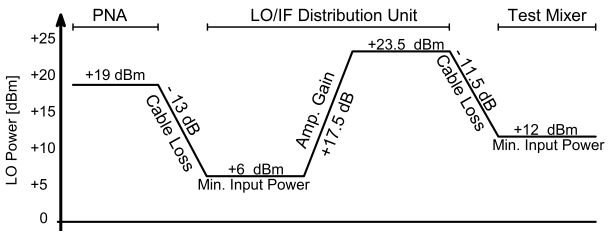

Fig. 7 Link-budget for the LO power distribution.

The maximum output from the VNA is +19 dBm at 10 GHz from port 3 which is used for source 2. The distribution unit required a minimum LO input of +6 dBm giving a maximum acceptable loss of 13 dB. The used LO cable (UTiFLEX UFB293C) has a loss of 0.59 dB/m at 10 GHz. This means that $^{13}/_{0.59} = 22$ meters of cable can be used from VNA to distribution unit and $^{11.5}/_{0.59} = 19.5$ meters of cable can be used from the distribution unit to the test mixer. In total, this gives an operational range of 41,5 meters when measuring at maximum 30 GHz. Lower measurement frequencies would result in a longer range and an optional LO amplifier would extend the range even farther. Alternatively an optical solution could be used for the distribution of the LO. This would allow for very long ranges due to the low loss introduced by fiber-optic cables. However, the cost of these systems is significant.

3 Used measurement system

The measurement system capabilities can be further extended to simultaneously record two complex channel frequency responses. The fundamental principle is though unchanged from the system presented in the previous section.

3.1 VNA based sounding system

A block diagram of the system is seen in Fig. 8, where the system is operating with two test mixers allowing for recording two individual complex channel frequency responses.

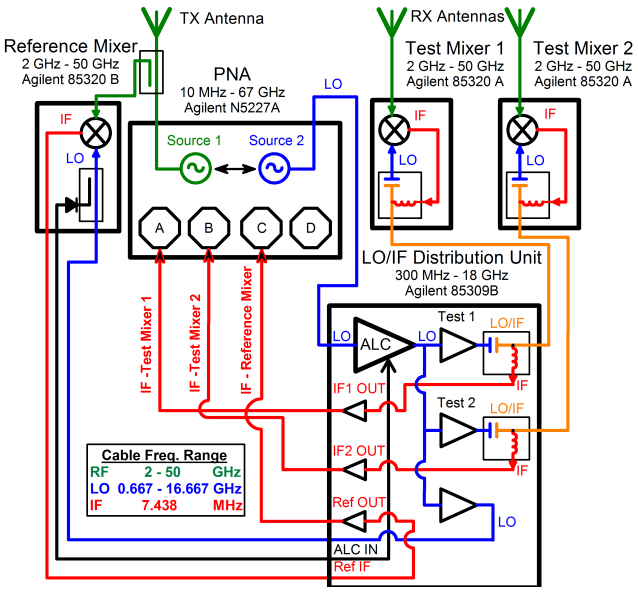

Fig. 8 Block diagram of the used sounding system. Green is RF frequency, blue is LO frequency and red is IF frequency.

Besides the two test mixers, the reference mixer is also used in this setup. This means that three frequency responses are recorded by the VNA on port A, B and C. The recorded frequency response from the reference mixer is used to decrease the impact of the unwanted frequency response of the measurement system. The reference frequency response is recorded just before the port of the transmitting antenna by using an RF coupler (Agilent 87301E). The signal from source 1 until the antenna port of the transmitting antenna can be written as:

$$Y_{TX}(f) = X(f)\,G(f) \tag{1}$$

where $X(f)$ is the signal from source 1 and $G(f)$ is the unwanted frequency response of the measurement system.

Then the received signal from test mixer 1 is recorded at port A and can be written as:

$$A(f) = X(f)\,G(f)\,H(f)\,G_{test}(f) \tag{2}$$

where $H(f)$ is the channel frequency response which we would like to measure and $G_{test}(f)$ is the unwanted frequency response of the test mixers RF chain.

In a similar way, the received signal from the reference mixer is recorded at port C and can be written as:

$$C(f) = X(f)\,G(f)\,G_{ref}(f) \tag{3}$$

where $G_{ref}(f)$ is the unwanted frequency response of the reference mixers RF chain.

Now by assuming that the frequency response of the test mixer RF chain is approximately the same as the one for the reference mixer the channel response can be found as:

$$H(f) = \frac{A(f)}{C(f)} \tag{4}$$

The assumption of the frequency response of the test mixer RF chain is approximately the same is justified via use of identical cabling and the fact that the system is normalized/calibrated from transmit antenna port to receiver antenna port before the measurement. The frequency response for test mixer 2 can be found in the same way as for test mixer 1.

For the used setup a horn antenna (Pasternack - PE9851/2F-10) is used at the transmit side (TX). The receive side (RX) is utilizing the possibility of recording two frequency responses by having both a horn (Flann - 22240-20) and a bi-conical antenna (AINFO - SZ-2003000/P). The reason for having a horn antenna and a bi-conical antenna as RX is to enable the use of both directional horn and virtual UCA for capturing the power-angle-delay profiles. Both the TX and RX antennas are connected via cables. The specifications of the used antennas are given together with the settings for the VNA in Table 1.

Table 1 Measurement System Setup

Parameter	Setting
Center Frequency	28 GHz
Bandwidth	4 GHz
Frequency Points	1500
TX power	15 dBm
TX antenna Azimuth HPBW	54°
TX antenna Elevation HPBW	53°
TX antenna gain	10 dBi
RX horn antenna Azimuth HPBW	22°
RX horn antenna Elevation HPBW	21°
RX horn antenna gain	18 dBi
RX bi-conical antenna gain	6 dBi

In Table 1 the transmit power is also given together with the antenna gains. Using this information an estimate of the RF range of the measurement system can be given. This range is given by the maximum allowed path loss defined as the loss of the transmitted power until the given sensitivity of the receiver. For the used measurement system, the maximum leveled output power from source 1 when sweeping from 26 to 30 GHz is 15 dBm and the sensitivity of the test mixer is -103 dBm. Together this leaves a maximum tolerable path loss of 118 dB. This can however be extended by applying high gain antennas.

The aim is to ensure a good dynamic range of the system and thereby high-quality measurements performed with it. The maximum range of the measurement system operating at 30 GHz was 41,5 meters. By using Friis free space propagation loss for LOS scenario and assuming a 10 dBi TX antenna gain together with a 6 dBi RX antenna gain, the received power can be calculated to -63.35 dB. This leaves a dynamic range from received power to the sensitivity level of 39.65 dB. The propagation loss is however highly dependent on the measurement scenario, e.g. Line-Of-Sight (LOS) or Non-LOS (NLOS). That is, the dynamic range in practice will be smaller.

3.2 Measurement Scenario

The measurement system was used an indoor scenario. The location is a laboratory located on the second floor on a contemporary building. A floor plan is shown in 9 and a picture of the laboratory is shown in Fig. 10.

In Fig. 9 the TX and RX positions are marked in relation to the surroundings. The aim of the selected

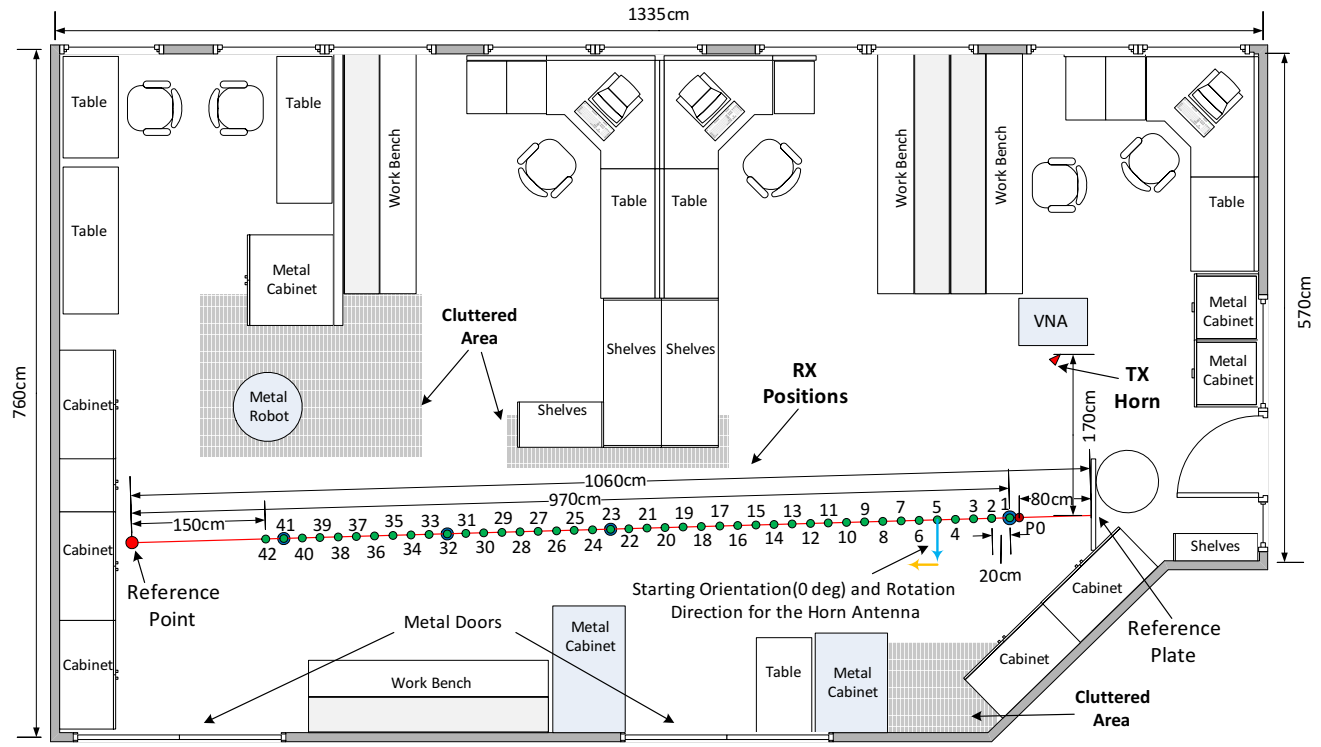

Fig. 9 Floor plan of the measurement scenario.

Fig. 10 View of the laboratory where the measurement was conducted

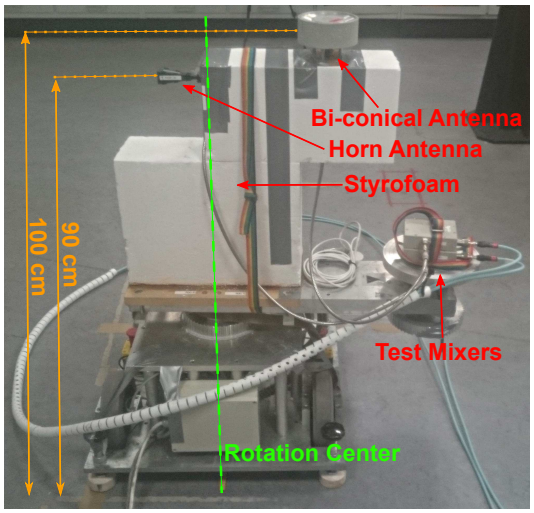

Fig. 11 Illustration of the receiver setup with turntable together with both horn and bi-conical antenna.

measurement locations together with the positioning of TX and RX is to be able to capture the change in PADP when the RX is moved farther away from the TX and from the LOS to the NLOS scenarios. For all the conducted measurements the TX antenna was oriented towards position RX-8 with a height of 100 cm. As seen in Fig. 9, a total of 42 RX positions (green) distributed with a 20 cm distance along a reference line (red) have been used. The RX positions are located such that the points starts in the LOS scenario and moves farther and farther in the NLOS scenario. To conduct the measurements at each RX position using both the horn and bi-conical antenna, a RX setup with a turntable as shown in Fig. 11 has been used.

As illustrated in Fig. 11, the horn antenna was placed in a height of 90 cm, with its main beam in the azimuth plane. The starting orientation (cyan) of the horn antenna at all the RX positions was orthogonal to the reference line as indicated at RX-5, in Fig. 9. The measurement at each RX position was conducted by rotating the horn antenna clockwise (orange) in the azimuth plane in steps of 1° using the turntable. For each ro-

tation step, a complex frequency response is recorded simultaneously for both horn and bi-conical antenna.

In Fig. 11 it can be seen that the bi-conical antenna is offset from the rotation center and placed above the horn antenna at a height of 100 cm, which is the same height as the TX antenna. The offset from the rotation center results in the bi-conical antenna forming a circle in the azimuth plane when the turntable is rotating as illustrated in Fig. 12.

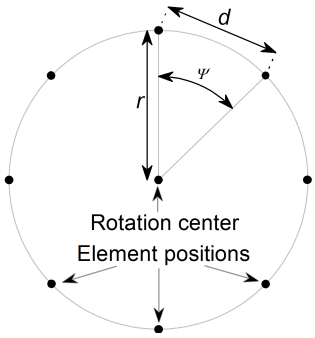

Fig. 12 Dimensions of the Uniform Circular Array (UCA).

The bi-conical antenna is moved around along the circle while a complex frequency response is recorded for each 1° (Ψ). This results in the possibility of forming a virtual UCA with 360 elements (N). To determine the needed offset from the rotation center (r) each element can be seen as a spatial sample of the channel. To avoid aliasing the distance (d) between these samples should be less than $\lambda/2$. The distance between points on the circle can be approximated by:

$$d \approx \frac{2\pi r}{N} \tag{5}$$

giving that:

$$\frac{2\pi r}{N} < \frac{\lambda}{2} \Rightarrow \; r < \frac{\lambda N}{4\pi} \;\; | \; N > 0 \wedge \lambda \in \mathbb{R} \tag{6}$$

From this, it can be seen that a solution is to minimize r. However, the obtainable angular resolution from the measurement conducted with the UCA increases with the aperture of the UCA, giving that r is wanted as large as possible. Due to this r has been chosen to be 25 cm, which give $d \approx 0.004$, with $\lambda/2 = 0.005$ at 30 GHz.

Each of the 42 complete 360° scans with steps of 1° in the azimuth plane while collecting the complex frequency response from both both horn and bi-conical antenna took roughly 6 minutes. During the time of each scan the scenario was completely static. The measurement of all the 42 RX positions was conducted during one night ensuring nothing was changed in the almost 6 hours the measurement took.

4 Measurement Results

In this section, the results from the measurement campaign are presented. First, we briefly explain the measured data for a representative LOS position and a NLOS position respectively. After that, we intend to investigate the channel dynamics over the measurement positions and frequency dependency of the channel characteristics.

4.1 Measured data in a LOS and in a NLOS scenario

To obtain the channel impulse repose (CIR), an inverse Fourier transformation (IFT) of the complex channel frequency response can be performed for each rotation step. A Hamming window has been applied to the data to suppress sidelobe levels. The resulting CIR for each rotation step can together with the orientation of the horn antenna be used to construct the power-angle-delay profile (PADP) for the azimuth plane, as seen in Fig. 13. The CIR from 360 positions of the bi-conical antenna can also be plotted in a similar way as seen in Fig. 14. It should be noted that the frequency response of the used antennas has not been removed from the recorded frequency sweeps and thus are embedded in the presented results.

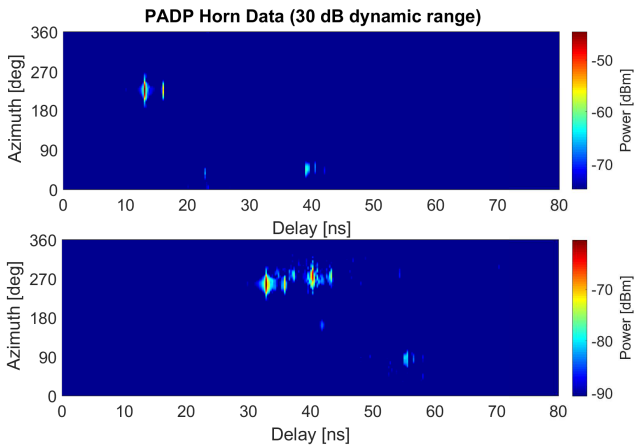

Fig. 13 Power-angle-delay profile using the horn antenna data. Position 8 is shown in the top and position 40 is shown in the bottom. Both locations have been plotted with 30 dB dynamic range.

In Fig. 13 and Fig. 14, position 8 and 40, shown in Fig. 9, have been used to illustrate a LOS and a NLOS case of the measurement scenario, respectively. The measured PADP is sparse and specular, with few paths detected both in LOS and NLOS scenarios. The CIR from the bi-conical antenna seen in Fig. 14 can not directly be related in angular domain. The delay

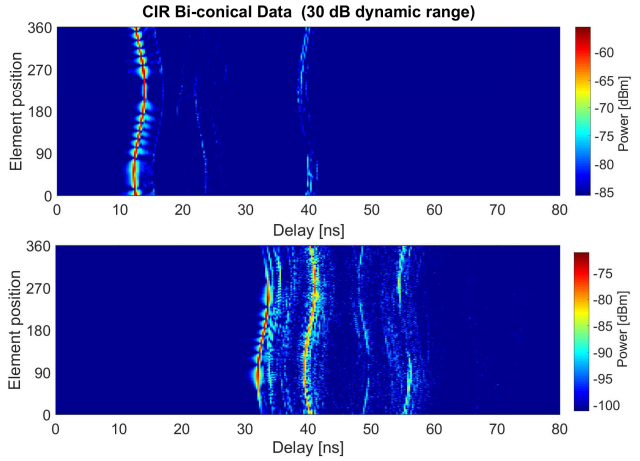

Fig. 14 Channel impulse response for the 360 positions of the bi-conical antenna data. Position 8 is shown in the top and position 40 is shown in the bottom. Both locations have been plotted with 30 dB dynamic range.

domain can, however, be compared to the components given by the horn data. In the LOS case, shown in the top of Fig. 14, the strongest component is located at roughly around 13 ns in delay which correspond to the horn data. The components in the NLOS case, shown in the bottom of Fig. 14, also correspond to the components seen from the horn data.

To be able to compare the data from the bi-conical antenna in the angular domain a UCA is formed. Then the PADP can be found by applying the maximum likelihood estimator with successive interference cancellation (MLE-SIC) with a wideband and spherical-wave signal model as described in [28]. The reason for applying a spherical-wave signal model to the MLE-SIC estimation is due to the size of the used UCA. The aperture of the UCA is 50 cm resulting in the far field assumption not being valid due to the vicinity of interacting object in the chosen scenario. In addition, the used ML-based estimator has the advantages of higher estimation resolution and less sidelobes interfering in the resultant PADP compared to spectrum-based estimators like delay-and-sum beamforming [13]. The resulting azimuth PADPs are presented in Fig. 15 for position 8 and in Fig. 16 for position 40, respectively.

The measured PADPs with the virtual UCA match well with the ones with the horn antenna, where detected multipath components with same angle and delay values are shown. Note that the power levels are different due to the difference in antenna gain of 12 dB between the horn and bi-conical antenna. The measured PADPs with the virtual UCA are used for later analysis since much higher angle resolution can be achieved for the virtual UCA with the maximum likelihood estimator.

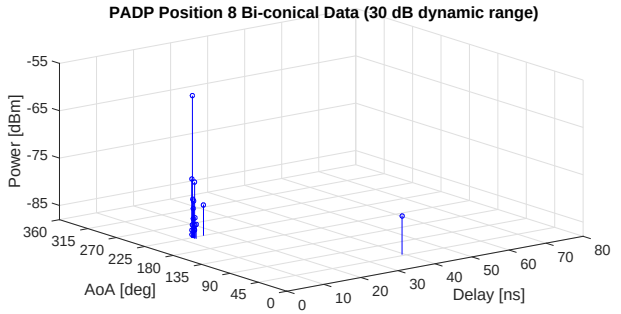

Fig. 15 Power-angle-delay profile using the bi-conical antenna data for position 8 with 30 dB dynamic range.

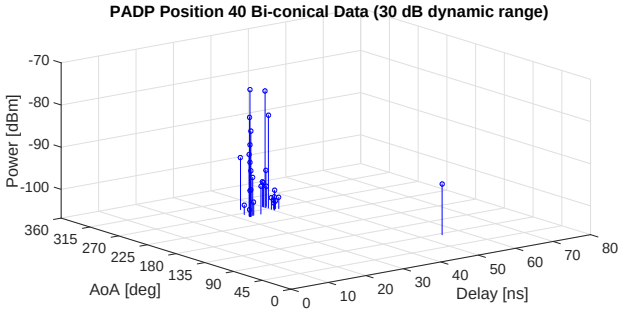

Fig. 16 Power-angle-delay profile using the bi-conical antenna data for position 40 with 30 dB dynamic range.

The path trajectory can be constructed based on the measured PADPs in the LOS and NLOS scenarios, as shown in Fig. 17 and Fig. 18 for measurement position 8 and 40, respectively.

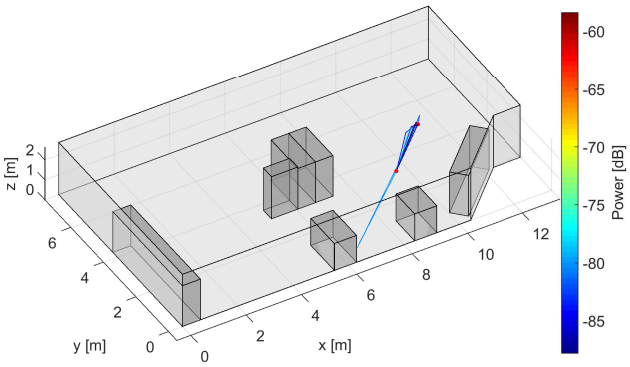

Fig. 17 Measurement based ray-Tracing for position 8 with 30 dB dynamic range. Red dot is RX and TX.

In the LOS case, shown in the top of Fig. 13, the strongest component is located at roughly 230° and 13 ns in delay. This corresponds to the direct LOS path between the TX and the RX. A secondary component is seen at 50° and 40 ns in delay which corresponds to a backscatter from the metal door behind the RX as seen from the TX. In the NLOS case, the strongest compo-

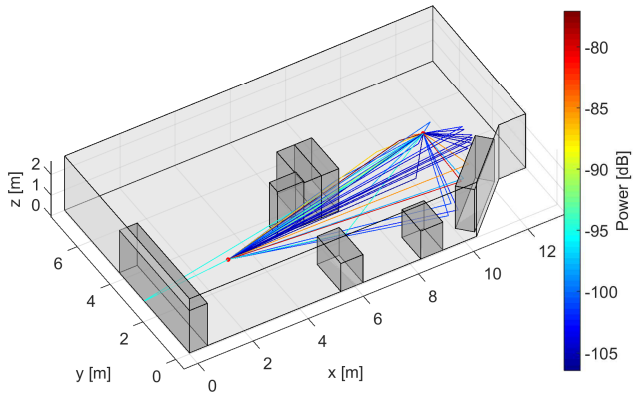

Fig. 18 Measurement based ray-Tracing for position 40 with 30 dB dynamic range. Red dot is RX and TX.

nent is located at 270° and 33 ns in delay which could correspond to a diffraction around the corner of the obstructing shelve seen in Fig. 9. Both position 8 in Fig. 17 and position 40 in Fig. 18 show the backscatter with significant longer delay as also seen in the horn data. As shown in Fig. 17 and Fig. 18, the path trajectories for the LOS and NLOS scenario differ significantly. This spatial dynamics of the channel is investigated further in the following section.

Given the fact that the two measured PADP present consistent results, it can be concluded that the channel sounding system is indeed capable of capturing two responses at the same time.

4.2 Spatial Dynamics

It is important to understand how the channel profiles vary over different measurement locations. One of the practical design challenges in beamforming schemes is how often the beamforming should be updated to identify the dominant paths in the channel. With a highly dynamic channel over spatial locations, a more frequent update is needed, which would increase system cost. To investigate the spatial dynamics of the measurements, all PADP have been calculated for all the 42 measurement positions using the MLE-SIC algorithm. The delay and angular domain results are plotted in two different plots for illustration purpose. The delay characteristics are presented in Fig. 19 and the angular characteristics in Fig. 20. From Fig. 19 and Fig. 20, it can be seen that the channels are sparse for most measurement points. In the LOS region (i.e. measurement positions from 1 to 11), LOS path is dominant. In the NLOS region, most paths are concentrated in an angle region.

The second order characteristics have also been calculated for all the measurement positions. The resulting

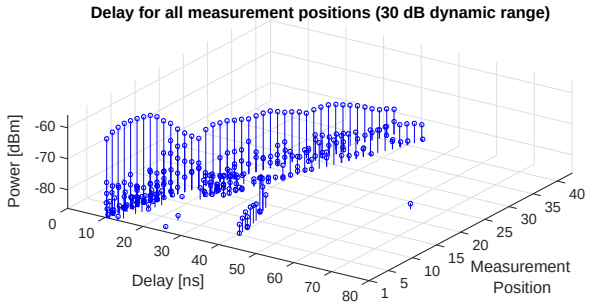

Fig. 19 Delay domain characteristics plotted for all measurement positions with 30 dB dynamic range.

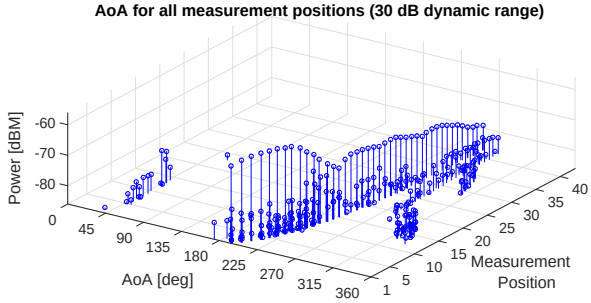

Fig. 20 Angular domain characteristics plotted for all measurement positions with 30 dB dynamic range.

delay and angular spread are shown in Fig. 21. In Fig. 21, it is clear that the region from measurement position 1 until 11 is dominated by a LOS component, which results in a low delay and angle spread. From measurement position 12 until 26 a transition zone is seen. Components from the surroundings have a larger impact, resulting in a larger spread. After measurement position 26 the spread decreases again as the surroundings might have a guiding effect towards the RX.

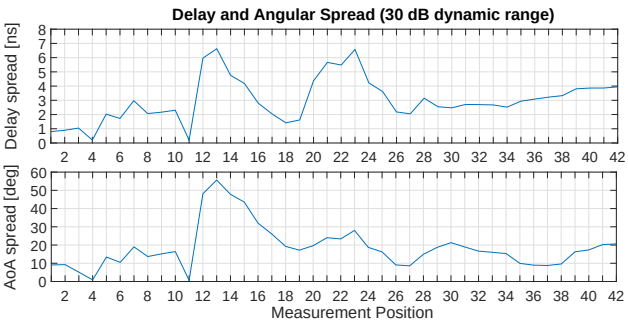

Fig. 21 Comparison of delay and angular spread for all measurement positions with 30 dB dynamic range.

5 Conclusion

This work presents the improvement of an existing VNA based measurement system operating in the frequency range from 2 to 50 GHz. A solution to address system instability at 2 to 4 GHz and 21 to 26.5 GHz is described. The measurement system is further extended to be capable of recording two independent channel frequency responses together with a reference frequency response. The proposed system is validated in the range from 2 to 30 GHz with a power drift of less than 0.5 dB in the whole span. The phase drift in the same span is less than 1° over a measurement period of 1 hour.

The proposed measurement system have been utilized for a measurement in the frequency range from 26 to 30 GHz. The measurements were conducted in both LOS and NLOS using 42 measurement positions distributed along a line through an indoor laboratory environment. Two channel frequency responses were recorded simultaneously using a directional horn antenna and a virtual uniform circular array. The recorded data is used to construct power-angular-delay profiles (PADP) and a comparison between the two showed good agreement. The PADP showed a sparse propagation environment when the dynamic range of the measurement was constrained to a 30 dB range. Plotting the recorded PADPs evolution over the 42 measurements positions showed it was possible to track dominant paths.

Acknowledgements The authors would like to thank the lab staff for valuable assistance with measurements.

References

1. P. Demestichas, A. Georgakopoulos, D. Karvounas, K. Tsagkaris, V. Stavroulaki, J. Lu, C. Xiong, and J. Yao, "5g on the horizon: Key challenges for the radio-access network," *Vehicular Technology Magazine, IEEE*, vol. 8, no. 3, pp. 47–53, Sept 2013.
2. Q. Li, H. Niu, A. Papathanassiou, and G. Wu, "5g network capacity: Key elements and technologies," *Vehicular Technology Magazine, IEEE*, vol. 9, no. 1, pp. 71–78, March 2014.
3. L. Wei, R. Q. Hu, Y. Qian, and G. Wu, "Key elements to enable millimeter wave communications for 5g wireless systems," *IEEE Wireless Communications*, vol. 21, no. 6, pp. 136–143, December 2014.
4. Ofcom, "Spectrum above 6 ghz for future mobile communications," Ofcom UK, Riverside House, 2a Southwark Bridge Road, London, Consultation Report, 2015.
5. S. Methley, W. Webb, S. Walker, and J. Parker, "Study on the suitability of potential candidate frequency bands above 6ghz for future 5g mobile broadband systems," Quotient Associates Limited, Compass House, Vision Park, Chivers Way Histon, Cambridge, CB24 9AD, UK, Technical Report, 2015.
6. ITU, *Attenuation by atmospheric gasess*, ITU-R P.676-10, Sep. 2013.
7. T. Rappaport, S. Sun, R. Mayzus, H. Zhao, Y. Azar, K. Wang, G. Wong, J. Schulz, M. Samimi, and F. Gutierrez, "Millimeter wave mobile communications for 5g cellular: It will work!" *Access, IEEE*, vol. 1, pp. 335–349, 2013.
8. T. Rappaport, F. Gutierrez, E. Ben-Dor, J. Murdock, Y. Qiao, and J. Tamir, "Broadband millimeter-wave propagation measurements and models using adaptive-beam antennas for outdoor urban cellular communications," *Antennas and Propagation, IEEE Transactions on*, vol. 61, no. 4, pp. 1850–1859, April 2013.
9. A. Sulyman, A. Nassar, M. Samimi, G. Maccartney, T. Rappaport, and A. Alsanie, "Radio propagation path loss models for 5g cellular networks in the 28 ghz and 38 ghz millimeter-wave bands," *Communications Magazine, IEEE*, vol. 52, no. 9, pp. 78–86, September 2014.
10. R. J. C. Bultitude, R. F. Hahn, and R. J. Davies, "Propagation considerations for the design of an indoor broadband communications system at ehf," *IEEE Transactions on Vehicular Technology*, vol. 47, no. 1, pp. 235–245, Feb 1998.
11. G. A. Kalivas, M. El-Tanany, and S. Mahmoud, "Millimeter-wave channel measurements with space diversity for indoor wireless communications," *IEEE Transactions on Vehicular Technology*, vol. 44, no. 3, pp. 494–505, Aug 1995.
12. H. Xu, T. S. Rappaport, R. J. Boyle, and J. H. Schaffner, "Measurements and models for 38-ghz point-to-multipoint radiowave propagation," *IEEE Journal on Selected Areas in Communications*, vol. 18, no. 3, pp. 310–321, March 2000.
13. W. Fan, I. C. Llorente, J. Nielsen, K. Olesen, and G. F. Pedersen, "Measured wideband characteristics of indoor channels at centimetric and millimetric bands," *EURASIP Journal on Wireless Communications and Networking*, vol. 2016, no. 1 -Special issue on Radio Channel models for higher frequency bands, 2016.
14. J. Nielsen and G. F. Pedersen, "Dual-polarized indoor propagation at 26 ghz," in *2016 IEEE 27th Annual International Symposium on Personal, Indoor, and Mobile Radio Communication (PIMRC)*, September 2016.
15. G. R. Maccartney, T. S. Rappaport, S. Sun, and S. Deng, "Indoor office wideband millimeter-wave propagation measurements and channel models at 28 and 73 ghz for ultra-dense 5g wireless networks," *IEEE Access*, vol. 3, pp. 2388–2424, 2015.
16. Y. Kim, H. Y. Lee, P. Hwang, R. K. Patro, J. Lee, W. Roh, and K. Cheun, "Feasibility of mobile cellular communications at millimeter wave frequency," *IEEE Journal of Selected Topics in Signal Processing*, vol. PP, no. 99, pp. 1–1, 2016.
17. W. Roh, J.-Y. Seol, J. Park, B. Lee, J. Lee, Y. Kim, J. Cho, K. Cheun, and F. Aryanfar, "Millimeter-wave beamforming as an enabling technology for 5g cellular communications: theoretical feasibility and prototype results," *Communications Magazine, IEEE*, vol. 52, no. 2, pp. 106–113, February 2014.
18. S. Han, C. l. I, Z. Xu, and C. Rowell, "Large-scale antenna systems with hybrid analog and digital beamforming for millimeter wave 5g," *IEEE Communications Magazine*, vol. 53, no. 1, pp. 186–194, January 2015.
19. A. F. Molisch, *Wireless communications*. IEEE Press, 2005, iSBN: 978-0-470-84888-3.

20. ——, "Ultrawideband propagation channels-theory, measurement, and modeling," *IEEE Transactions on Vehicular Technology*, vol. 54, no. 5, pp. 1528–1545, Sept 2005.
21. J. O. Nielsen, J. B. Andersen, P. C. F. Eggers, G. F. Pedersen, K. Olesen, and H. Suda, "Measurements of indoor 16 times;32 wideband mimo channels at 5.8 ghz," in *Eighth IEEE International Symposium on Spread Spectrum Techniques and Applications*, Aug 2004, pp. 864–868.
22. T. S. Rappaport, G. R. MacCartney, M. K. Samimi, and S. Sun, "Wideband millimeter-wave propagation measurements and channel models for future wireless communication system design," *IEEE Transactions on Communications*, vol. 63, no. 9, pp. 3029–3056, Sept 2015.
23. X. Chen, S. Liu, J. Lu, P. Fan, and K. B. Letaief, "Smart channel sounder for 5g iot: From wireless big data to active communication," *IEEE Access*, vol. 4, pp. 8888–8899, 2016.
24. S. Salous, S. M. Feeney, X. Raimundo, and A. A. Cheema, "Wideband mimo channel sounder for radio measurements in the 60 ghz band," *IEEE Transactions on Wireless Communications*, vol. 15, no. 4, pp. 2825–2832, April 2016.
25. X. Raimundo, S. Salous, and A. A. Cheema, "Indoor radio propagation measurements in the v-band," in *Radio Propagation and Technologies for 5G (2016)*, Oct 2016, pp. 1–5.
26. W. Fan, I. C. Llorente, and G. F. Pedersen, "Comparative study of centimetric and millimetric propagation channels in indoor environments," in *2016 10th European Conference on Antennas and Propagation (EuCAP 2016)*, April 2016.
27. J. Hejselbaek, W. Fan, and G. F. Pedersen, "Ultrawideband vna based channel sounding system for centimetre and millimetre wave bands," in *2016 IEEE 27th Annual International Symposium on Personal, Indoor, and Mobile Radio Communications (PIMRC)*, Sept 2016, pp. 1–6.
28. Y. Ji, W. Fan, and G. Pedersen, "Channel estimation for wideband large-scale array systems with a spherical-wave model," 2017, submitted to IEEE transaction on Vehicular Technology.